Height-finding for automotive THz radars

Shishanov, Sergei; Bystrov, Aleksandr; Hoare, Edward; Stove, Andrew; Gashinova, Marina; Cherniakov, Mikhail; Tran, Thuy-Yung; Clarke, Nigel

DOI:
10.1109/TITS.2018.2845542

Document Version
Peer reviewed version

Citation for published version (Harvard):
Shishanov, S, Bystrov, A, Hoare, E, Stove, A, Gashinova, M, Cherniakov, M, Tran, T-Y & Clarke, N 2019, 'Height-finding for automotive THz radars', *IEEE Transactions on Intelligent Transportation Systems* , vol. 20, no. 3, pp. 1170 - 1180. https://doi.org/10.1109/TITS.2018.2845542

Height-Finding for Automotive THz Radars

Sergei Shishanov, Aleksandr Bystrov, Edward G. Hoare, *Senior Member, IEEE*, Andrew Stove, *Senior Member, IEEE*, Marina Gashinova, Mikhail Cherniakov, Thuy-Yung Tran, and Nigel Clarke

***Abstract*— This paper explores radar methods to measure the coordinates (distance and height) of objects on or beside a road. Knowledge of these parameters is essential in the development of autonomous or semi-autonomous cars, as well as to improve driving safety. It is shown that the height is best found by trilateration from sensors at multiple locations on a vehicle. The novelty of the work consists in the formulation of the problem and in its solution using a low-THz radar trilateration approach. The expressions obtained allow calculating the coordinates of targets using a number of different methods of radar trilateration. The influence of the system parameters on the accuracy of measurement using different methods of trilateration has been analyzed. The assumptions made were verified by the experimental system based on a 300-GHz ultra-wideband radar. Experimental results are in good agreement with theoretical calculations; they confirmed the practicality of obtaining high-accuracy height measurements on distributed targets such as pedestrians. The physical basis of the techniques developed would also allow the plan position of a target to be found using the same approach.**

***Index Terms*— Automotive applications, radar remote sensing, radar imaging, radar measurements.**

I. Introduction

CURRENT research explores the prospects for a new generation of sensor systems that will be mounted in vehicles to enhance the safety of driving. The sensors, small enough to be mounted unobtrusively on vehicles, will allow high-resolution images to be produced in real time that can be interpreted by intelligent vehicle systems to determine appropriate actions in hazardous circumstances. The main research work activities in this study relate to the measurement of the position on the horizontal plane of objects on or near the road (these objects in the document will also be called targets), and to measure the dimensions of the objects in the vertical plane. The examples of such objects are pedestrians, speed bumps, as well as random obstacles such as holes in the road, rocks or fallen trees.

Recent studies prove that technologies like collision detection, lane departure warning, adaptive cruise control and autonomous emergency braking help to reduce accidents [1]. If an accident is unavoidable, modern in-car safety features like advanced airbags, smart seat belts and high-strength steel construction help to minimize injuries. That makes cars safer for drivers and passengers, but doesn't do anything to improve the survivability of car and pedestrian impacts [2]. That makes pedestrian (and animal) detection the next big wave in auto safety, especially since upcoming Euro NCAP standards will rate cars on their ability to prevent pedestrian injuries.

In recent years there have been many papers on pedestrian recognition using automotive radar [2]–[6]. The general approach to recognition is the extraction of the reflected signal parameters, followed by the use of classification algorithms [3]. In [2] and [4] pedestrian recognition by analyzing the motion pattern of a walking human using 24 GHz pulse Doppler radar was investigated. In [5] and [6] the pedestrian recognition was based on micro Doppler signature and on intensity image of the radar signal, reflected by a pedestrian was considered. Under optimal conditions over 95% of pedestrians were classified correctly using 77 GHz narrow-beam radar.

The availability of information on the height and distance of the object as well as its azimuth position will significantly increase the reliability of recognition of different road objects, including pedestrians. The position in the horizontal plane can be determined either by using a narrow azimuth beam and range measurements or it could be obtained by trilateration.

Like many sonar systems and some lower-frequency radar systems, the proposed THz imaging produces information, in this case height, by comparing measurements across an array of sensors [7], [8]. A fully-filled array of sensors would have to be very dense, since the distance between sensors must be proportional to wavelength if ambiguities (grating lobes) are to be avoided. The array can, however, be 'thinned' to only two or three elements if only a few targets will be present in any range-azimuth-Doppler cell.

Radar sensors are continuously improved to get better performance and resolve details of the targets, that could not be seen so far [3]. The high bandwidths available when using low-THz frequencies make it possible to distinguish between more closely spaced features in the reflected signal.

Manuscript received June 7, 2017; revised November 24, 2017 and April 6, 2018; accepted May 18, 2018. This work was supported by Jaguar Land Rover. The Associate Editor for this paper was Y. Gao. *(Corresponding author: Aleksandr Bystrov.)*

S. Shishanov is with Nizhny Novgorod State Technical University n.a. R.E. Alekseev, 603 950 Nizhny Novgorod, Russia (e-mail: shishanovsergey@gmail.com).

A. Bystrov, E. G. Hoare, A. Stove, M. Gashinova, and M. Cherniakov are with the University of Birmingham, Birmingham B15 2TT, U.K. (e-mail: a.bystrov@bham.ac.uk; e.g.hoare@bham.ac.uk; a.stove@bham.ac.uk; m.s.gashinova@bham.ac.uk; m.cherniakov@bham.ac.uk).

T.-Y. Tran and N. Clarke are with Jaguar Land Rover Automotive PLC, Coventry CV3 4LF, U.K. (e-mail: ttran3@jaguarlandrover.com; nclarke2@jaguarlandrover.com).

Color versions of one or more of the figures in this paper are available online at http://ieeexplore.ieee.org.

Digital Object Identifier 10.1109/TITS.2018.2845542

At the same time, waves in this band are not susceptible to complete obscuration by road dirt or precipitation, as infrared and optical systems would be.

To generate the required images, low THz waves must be transmitted from the vehicle, propagate through the surrounding environment and be scattered from objects and surfaces. Scattered waves propagating back to the vehicle and received by the sensor antennas provide the information required to form an image. The method of measuring the target coordinates is based on trilateration methods when the target is located by automatic trigonometric solution of the triangle composed of two (or more) transceivers and the target. This technique is a special case of a general multilateration method [9]. As it was showed in [10], trilateration technique cannot accurately estimate the position of a target if the distance measurements are too noisy. A possible solution is to increase the number of transceivers and include distance measurements from multiple sensors.

Whilst conventional 'thinned' arrays use phase comparison (interferometry) to estimate the targets' cross-range positions, at low-THz frequencies the bandwidths, and consequent high-range resolutions available, combined with the relatively short ranges, make time-difference of arrival (TDOA) techniques practical and attractive.

The paper is devoted to measuring the height of objects in a two-coordinate radar system. However, the results obtained can be generalized for a three-coordinate radar system. In this system the geometric dimensions of the objects can estimated.

The remainder of this paper is organized as follows. Section II will look at what is possible from a single sensor location, In this case the high range resolution can 'convert' differences in height to differences in range, but the accuracy which can be obtained is only marginal. Section III will look at various methods of radar trilateration are analyzed and expressions are obtained for the estimation of target coordinates. The theoretical measurement accuracy achievable with the use of these methods is investigated in Section IV. Issues relating to the interpolation of the signal envelope and filtering the ghost targets are considered in Section V. In Section VI the experimental results obtained using a point target are shown. Experimental results for distributed targets are presented in Section VII. Finally, the conclusions are formulated in Section VIII.

II. Height Estimation With a Single Sensor

The goal of this section is to estimate what signal parameters allow separation of two reflection points with different heights, located at the same horizontal distance from the sensor, when measurements are made from a sensor at a single location.

In Fig. 1 the geometry of measurements is shown: h_1 and h_2 are heights of the reflection points 1 and 2, where h_2 is a height of the highest reflection point of a target, $\delta_H = h_2 - h_1$is the height resolution, $\delta_R = r_2 - r_1$ is the range resolution, r_G is the horizontal (ground) distance between the radar and the target, r_1 and r_2 are slant ranges between transceiver positions and reflection points.

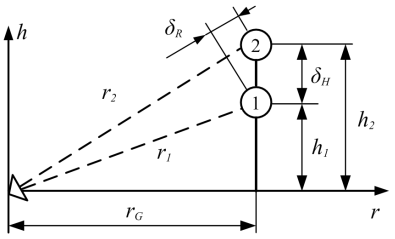

Fig. 1. The geometry of measurements.

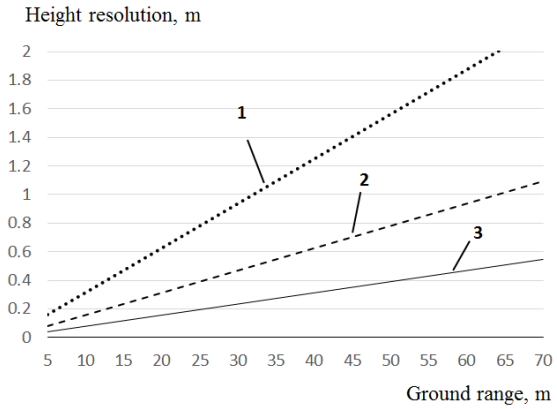

Fig. 2. The height resolution for different range and bandwidth 1 – 4 GHz, 2 – 8 GHz and 3 – 16 GHz.

At large distances, when $r_G \gg \delta_R$, the height resolution can be found from the approximate equation:

$$\frac{\delta_R}{\delta_H} \approx \frac{h_2}{r_2} \tag{1}$$

where $r_2 = \sqrt{r_G^2 + h_2^2}$. The solution of (1) has the form:

$$\delta_H = \delta_R \sqrt{1 + r_G^2 / h_2^2}. \tag{2}$$

From (2) it follows, that at larger distances height resolution is coarser than the range resolution and therefore in order to achieve the good height resolution it is necessary to use wideband signals.

As is well known, the range resolution of the radar depends on the bandwidth of the transmitted signal ΔF:

$$\delta_R \approx \frac{c}{2\Delta F}. \tag{3}$$

Therefore 4 GHz bandwidth corresponds to a range resolution of about 3.75 cm, 8 GHz to about 1.9 cm and 16 GHz to just under 1 cm.

In Fig. 2 the height resolution calculated by the equations (2) and (3) is shown in the case of detecting the pedestrian with a height of 1.8 m. The zero of a vertical scale is the height of the transceiver mounted on a vehicle bumper (the height over the surface is 0.6 m), therefore in this case $h_2 = 1.8 - 0.6 = 1.2$m.

As can be seen from the figure, in order to measure the height of a pedestrian at a distance over 50 meters, the signal bandwidth should be 8 GHz or higher.

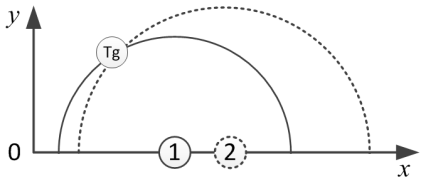

Fig. 3. Illustration of a trilateration principle: 1 and 2 – sensor locations, semicircles are position lines, the intersection point is a target Tg location.

This means that although height-finding with a single sensor is probably possible, it is at the edge of what is feasible, giving, even in theory, only just-adequate resolution at just-adequate range with the maximum plausible bandwidth.

III. Coordinates Estimation by Trilateration

To estimate the coordinates of the reflector in the horizontal plane along the abscissa and ordinate axes we should make measurements from at least two transceiver positions [11]. Each measurement is a time delay between the transmitted signal and the received signal, reflected from the target. A similar approach can be applied to the measurement of the coordinates of the reflector in the vertical plane.

Assuming a radar system with two sensors and a single target, the method is illustrated in Fig. 3. Each sensor measures the distance to the target separately. For the given case, the result, i.e. set of possible target locations for one sensor, is a circle around the sensor, with a radius given by the measured distance. For automotive radar the view will be limited to half-plane, so that the circles can be drawn as semicircles. Combining both semicircles yields a single point for the ideal case of infinite precision. The lines of equal distance are circles, therefore further this method we will call 'two circles'. Fig. 3 illustrates a classical 2D triangulation example. However, when the sensor array is vertically arranged, the ordinate x may be considered as the height of the object and in this case the trilateration refer to 3D problem.

In practice, because of radar finite range resolution, the result is an intersection area instead of intersection point. Within this area the target may be located at any point. The size of this area depends on the signal parameters, sensors configuration, distance to the target, signal to noise ratio, etc.

In multiple targets environment, we can potentially detect both real and 'phantom' targets, which arise from erroneous correlations between the detections seen at the different locations. This can also be appreciated by looking at the intersection between the lines of constant range corresponding to the different targets. In Fig. 4 the occurrence of a phantom target mark is illustrated. In the figure two sensors and two targets are shown. This configuration yields three intersections of the circles, all intersection points are possible target locations.

Our goal is to distinguish real targets from phantom. An additional method can be used for ambiguity resolution and the coordinates should be estimated by two methods. The correct target coordinates are equal in both methods; false marks are different [12]. Other trilateration methods require measurements from three transceivers to estimate the coordinates of reflectors.

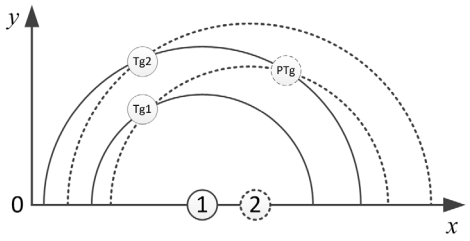

Fig. 4. Radar trilateration in multiple targets environment: 1 and 2 – sensor locations, semicircles are position lines, the intersection points Tg1 and Tg2 are targets and PTg is a phantom target.

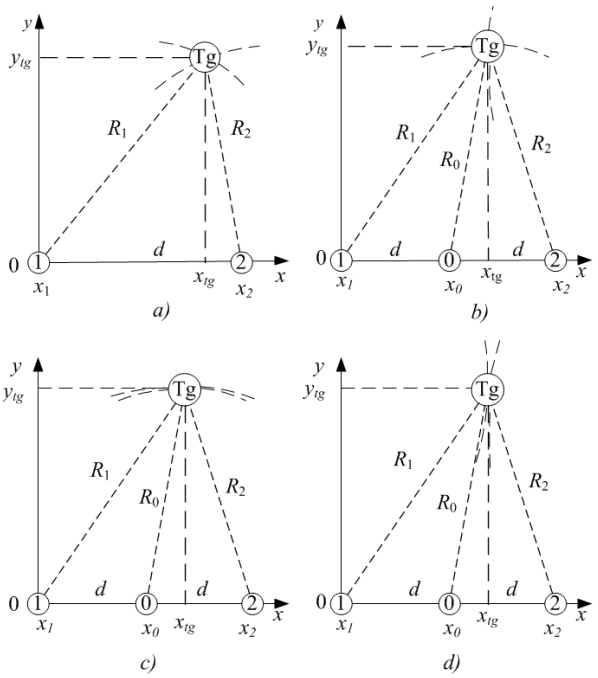

Fig. 5. Geometry of the system with two and three transceivers in different methods: (a) 'two circles', (b) 'circle and hyperbola', (c) 'circle and ellipse', and (d)'two hyperbolas'; 0, 1, and 2 are the transceiver positions; x_0, x_1, and x_2 are the transceiver position abscissae, d is the distance between transceiver positions (baseline), Tg is the target, x_{tg} and y_{tg} are the target coordinates (abscissa and ordinate), R_0, R_1 and R_2 are ranges between transceiver positions and a target.

In Fig. 5a–Fig. 5d the geometry of the system with two or three transceiver positions along with the important measurement parameters is shown.

The coordinates can be obtained using [11]:

- Range measurement from two positions, when the lines of equal distance are circles (see Fig. 5a);
- Differential range measurement from two side positions (the line of equal distance is hyperbola) and range measurement from the central position (circle), shown in Fig. 5b;
- The sum of ranges measurements from two side positions (ellipse) and range measurement from the central position (circle)), shown in Fig. 5c;
- Two differential range measurements (hyperbolas) from the left and central positions and the right and central positions, shown in Fig. 5d.

Note that for the circle/circle case both 'locations' need to both transmit and receive, although they do not need to (and in fact should not) pick up each other's signals.

In the other three cases one location needs to transmit and the others need only to receive, for the 'circle and ellipse' and the 'circle and hyperbola' the transmitting location also has to be able to receive, but for the 'two hyperbolas' case this is not necessary.

The target coordinates in the first 'two circles' method are defined by the following (see Fig.5a):

$$x_{tg} = \frac{R_1^2 + d^2 - R_2^2}{2 \cdot d}$$
$$y_{tg} = \sqrt{\left(R_1^2 - \left(\frac{R_1^2 + d^2 - R_2^2}{2 \cdot d}\right)^2\right)}. \quad (4)$$

Coordinates of the target in methods with three transceivers can be obtained by solving the system of equations:

$$\begin{cases} A_1 \cdot x^2 + A_2 \cdot x + A_3 \cdot y^2 + A_4 \cdot y + A_5 \cdot x \cdot y + A_6 = 0, \\ B_1 \cdot x^2 + B_2 \cdot x + B_3 \cdot y^2 + B_4 \cdot y + B_5 \cdot x \cdot y + B_6 = 0. \end{cases} \quad (5)$$

Coefficients A_1, A_2, A_3, A_4, A_5, A_6, B_1, B_2, B_3, B_4, B_5 and B_6 are determined by the type of the curve. Let's multiply the first equation from (5) by B_1, the second equation by A_1, and then subtract the first equation from the second equation:

$$C_1 \cdot y^2 + C_2 \cdot x + C_3 \cdot y + C_4 \cdot x \cdot y + C_5 = 0, \quad (6)$$

In (6): $C_1 = A_3 \cdot B_1 - B_3 \cdot A_1$, $C_2 = A_2 \cdot B_1 - B_2 \cdot A_1$, $C_3 = A_4 \cdot B_1 - B_4 \cdot A_1$, $C_4 = A_5 \cdot B_1 - B_5 \cdot A_1$, and $C_5 = A_6 \cdot B_1 - B_6 \cdot A_1$. From (6) we can obtain x as:

$$x = \frac{-y^2 \cdot C_1 - y \cdot C_3 - C_5}{C_2 + y \cdot C_4}. \quad (7)$$

The coordinate y of the intersection points of the curves can be obtained by solving the equation (8), which is obtained from using both equation (7) and the first equation from (5):

$$D_1 \cdot y^4 + D_2 \cdot y^3 + D_3 \cdot y^2 + D_4 \cdot y + D_5 = 0, \quad (8)$$

where:

$$\begin{aligned} D_1 &= A_1 \cdot C_1^2 + A_3 \cdot C_4^2 - A_5 \cdot C_1 \cdot C_4; \\ D_2 &= 2 \cdot A_1 \cdot C_1 \cdot C_3 - A_2 \cdot C_1 \cdot C_4 - 2 \cdot A_3 \cdot C_4 \cdot C_2 \\ &\quad + A_4 \cdot C_4^2 - A_5 \cdot C_1 \cdot C_2 - A_5 \cdot C_3 \cdot C_4; \\ D_3 &= 2 \cdot A_1 \cdot C_1 \cdot C_5 - A_2 \cdot C_1 \cdot C_2 + A_1 \cdot C_3^2 \\ &\quad - A_2 \cdot C_3 \cdot C_4 + A_3 \cdot C_2^2 + 2 \cdot A_4 \cdot C_2 A_5 \cdot C_2 \cdot C_3 \\ &\quad - A_5 \cdot C_4 \cdot C_5 + A_6 \cdot C_4^2, \\ D_4 &= 2 \cdot A_1 \cdot C_3 \cdot C_5 - A_2 \cdot C_2 \cdot C_3 - A_2 \cdot C_4 \cdot C_5 + A_4 \cdot C_2^2 \\ &\quad - A_5 \cdot C_2 \cdot C_5 + 2 \cdot A_6 \cdot C_2 \cdot C_4; \\ D_5 &= A_1 \cdot C_5^2 - A_2 \cdot C_2 \cdot C_5 + A_6 \cdot C_2^2. \end{aligned}$$

Equation (8) can be solved by general formulas for root of equation of the 4-th degree. We can start the simplification of (8) by assuming, without loss of generality that the sensors are placed along one of the coordinate axes (for example x). The central sensor can likewise be placed in the origin of coordinates; in a practical case, the distance between sensors can also be made equal.

The equation of circle for 'circle and hyperbola' curves is defined by the following:

$$x^2 + y^2 - R_0^2 = 0. \quad (9)$$

The equation of hyperbola for 'circle and hyperbola' curves is defined by the following:

$$b^2 x^2 - a^2 y^2 - a^2 b^2 = 0, \quad (10)$$

where $a = (R_1 - R_2)/2 = \Delta R/2$ and $b = a\sqrt{(d/a)^2 - 1}$.

Using both equations (9) and (10) the solution for 'circle and hyperbola' curves (11) is defined by the following:

$$x_{tg} = \pm\sqrt{R_0^2 - y_{tg}^2}$$
$$y_{tg} = \frac{1}{d}\sqrt{d^2 \cdot R_0^2 - R_0^2 \cdot \left(\frac{\Delta R}{2}\right)^2 - \left(\frac{\Delta R}{2}\right)^2 \cdot d^2 + \left(\frac{\Delta R}{2}\right)^4}, \quad (11)$$

The circle in 'circle and ellipse' method is defined by (9) and ellipse is defined by the following:

$$b^2 x^2 + a^2 y^2 - a^2 b^2 = 0, \quad (12)$$

where $a = (R_1 + R_2)/2 = R_\Sigma/2$ and $b = a\sqrt{1 - (d/a)^2}$.

Using both equations (9) and (12) the solution for 'circle and hyperbola' curves is defined by the following:

$$x_{tg} = \pm\sqrt{R_0^2 - y_{tg}^2}$$
$$y_{tg} = \frac{1}{d}\sqrt{d^2 \cdot R_0^2 - R_0^2 \cdot \left(\frac{R_\Sigma}{2}\right)^2 - \left(\frac{R_\Sigma}{2}\right)^2 \cdot d^2 + \left(\frac{R_\Sigma}{2}\right)^4}, \quad (13)$$

The first hyperbola in 'two hyperbolas' method is defined by the following:

$$b_1^2 \left(x + d/2\right)^2 - a_1^2 y^2 - a_1^2 b_1^2 = 0, \quad (14)$$

where $a_1 = (R_1 - R_0)/2 = \Delta R_1/2$ and $b_1 = a_1\sqrt{\left(\frac{d}{2a_1}\right)^2 - 1}$.

The second hyperbola in the 'two hyperbolas' method is defined by the following:

$$b_2^2 \left(x - d/2\right)^2 - a_2^2 y^2 - a_2^2 b_2^2 = 0, \quad (15)$$

where $a_2 = (R_2 - R_0)/2 = \Delta R_2/2$ and $b_2 = a_2\sqrt{\left(\frac{d}{2a_2}\right)^2 - 1}$.

Using both equations (14) and (15) the solution for 'two hyperbolas' curves (8) is defined by the following:

$$x_{tg\,1,2} = \frac{k}{2} \pm \sqrt{\frac{k^2}{4} - \left(\frac{d^2}{4} - \frac{\Delta R_1^2 \Delta R_2^2}{4d^2}\right)}$$
$$y_{tg\,1,2,3,4} = \pm\sqrt{\left(\frac{d^2}{\Delta R_1^2} - 1\right)\left(x_{tg\,1,2}^2 - x_{tg\,1,2} d + \frac{\Delta R_1^2}{4}\right)}, \quad (16)$$

where $k = \frac{d^2 \Delta R_1^2 - 2\Delta R_1^2 \Delta R_2^2 + \Delta R_2^2 d^2}{d(\Delta R_1^2 - \Delta R_2^2)}$.

IV. Accuracy of Measurements

In order to estimate the accuracy of coordinate measurement we have calculated root mean square errors in the case of a point target. In each case the Cartesian coordinates are derived from two range measurements, ξ_1 and ξ_2. The errors on these range measurements are independent and we assumed that their errors have a normal distribution with zero mean. Solutions for the standard deviation of a coordinate estimation can be defined by the following:

$$\sigma_x = \sqrt{\left(\frac{\partial x}{\partial \xi_1}\right)^2 \sigma_{\xi_1}^2 + \left(\frac{\partial x}{\partial \xi_2}\right)^2 \sigma_{\xi_2}^2},$$
$$\sigma_y = \sqrt{\left(\frac{\partial y}{\partial \xi_1}\right)^2 \sigma_{\xi_1}^2 + \left(\frac{\partial y}{\partial \xi_2}\right)^2 \sigma_{\xi_2}^2}. \tag{17}$$

where $\partial x/\partial\xi_1$, $\partial x/\partial\xi_2$, $\partial y/\partial\xi_1$, and $\partial y/\partial\xi_2$ are partial derivatives for x and y on measurements ξ_1 and ξ_2, σ_{ξ_1} and σ_{ξ_2} are root mean square errors of original range estimates. Equations (17) were obtained from equations (4), (11), (13), and (16) by performing a Taylor series expansion about a true value using the first derivative [13].

A. Accuracy of 'Two Circles' Method

In 'two circles' method the measurements ξ_1 and ξ_2 are the range measurements: $\xi_1 = R_1$, $\xi_2 = R_2$. Then $\sigma_{\xi_1} = \sigma_{\xi_2} = \sigma_R = c\cdot\sigma_\tau/2$, where c is the speed of light, $\sigma_\tau = 1/(q\cdot\Delta\omega_{\text{eff.}})$ defines the potential accuracy of time measurements, $q = \sqrt{2\cdot E/N_0}$ is determined by signal energy E and noise power spectral density N_0, $\Delta\omega_{\text{eff.}}$ is the effective signal baseband. The solutions $\partial x/\partial\xi_1$, $\partial x/\partial\xi_2$, $\partial y/\partial\xi_1$, and $\partial y/\partial\xi_2$ for 'two circles' method are defined by the following:

$$\frac{\partial x_{tg}}{\partial R_1} = \frac{R_1}{d},$$
$$\frac{\partial x_{tg}}{\partial R_2} = -\frac{R_2}{d},$$
$$\frac{\partial y_{tg}}{\partial R_1} = \frac{2R_1 - R_1\frac{\left(d^2+R_1^2-R_2^2\right)}{d^2}}{2\sqrt{R_1^2 - \frac{\left(d^2+R_1^2-R_2^2\right)^2}{4d^2}}},$$
$$\frac{\partial y_{tg}}{\partial R_2} = \frac{R_2\frac{\left(d^2+R_1^2-R_2^2\right)}{d^2}}{2\sqrt{R_1^2 - \frac{\left(d^2+R_1^2-R_2^2\right)^2}{4d^2}}}. \tag{18}$$

B. Accuracy of the 'Circle and Hyperbola' Method

In 'circle and hyperbola' method, the measurements ξ_1 and ξ_2 are the differential range ΔR and range measurement R_0: $\xi_1 = R_0$, $\xi_2 = \Delta R = R_1 - R_2$. Then $\sigma_{\xi_1} = \sigma_R = c\cdot\sigma_\tau/2$ and $\sigma_{\xi_2} = \sigma_R\sqrt{2} = c\cdot\sigma_\tau/\sqrt{2}$. The solutions $\partial x/\partial\xi_1$, $\partial x/\partial\xi_2$, $\partial y/\partial\xi_1$, and $\partial y/\partial\xi_2$ for 'circle and hyperbola' method are defined by the following:

$$\frac{\partial y_{tg}}{\partial R_0} = \frac{R_0\left(4d^2 - \Delta R^2\right)}{d\sqrt{16\,d^2R_0^2 - 4R_0^2\Delta R^2 - 4d^2\Delta R^2 + \Delta R^4}},$$
$$\frac{\partial y_{tg}}{\partial \Delta R} = \frac{-\Delta R R_0^2 - \Delta R d^2 + \Delta R^3/2}{d\sqrt{16\,d^2R_0^2 - 4R_0^2\Delta R^2 - 4d^2\Delta R^2 + \Delta R^4}},$$
$$\frac{\partial x_{tg}}{\partial R_0} = \pm\frac{R_0 - y_{tg}\frac{\partial y_{tg}}{\partial R_0}}{\sqrt{R_0^2 - y_{tg}^2}},$$
$$\frac{\partial x_{tg}}{\partial \Delta R} = \pm\frac{-y_{tg}\frac{\partial y_{tg}}{\partial \Delta R}}{\sqrt{R_0^2 - y_{tg}^2}}. \tag{19}$$

C. Accuracy of the 'Circle and Ellipse' Method

In 'circle and ellipse' method, the measurements ξ_1 and ξ_2 are the summary range R_Σ and range measurement R_0: $\xi_1 = R_0$, $\xi_2 = R_\Sigma = R_1 + R_2$. Then $\sigma_{\xi_1} = \sigma_R = c\cdot\sigma_\tau/2$ and $\sigma_{\xi_2} = \sigma_R\sqrt{2} = c\cdot\sigma_\tau/\sqrt{2}$. The solutions $\partial x/\partial\xi_1$, $\partial x/\partial\xi_2$, $\partial y/\partial\xi_1$, and $\partial y/\partial\xi_2$ for 'circle and ellipse' method are defined by the following:

$$\frac{\partial x_{tg}}{\partial R_0} = \pm\frac{R_0 - y_{tg}\frac{\partial y_{tg}}{\partial R_0}}{\sqrt{R_0^2 - y_{tg}^2}},$$
$$\frac{\partial x_{tg}}{\partial R_\Sigma} = \pm\frac{-y_{tg}\frac{\partial y_{tg}}{\partial R_\Sigma}}{\sqrt{R_0^2 - y_{tg}^2}}.$$
$$\frac{\partial y_{tg}}{\partial R_0} = \frac{R_0\left(4d^2 - R_\Sigma^2\right)}{d\sqrt{16\,d^2R_0^2 - 4R_0^2R_\Sigma^2 - 4d^2R_\Sigma^2 + R_\Sigma^4}},$$
$$\frac{\partial y_{tg}}{\partial R_\Sigma} = \frac{-R_\Sigma R_0^2 - R_\Sigma d^2 + R_\Sigma^3/2}{d\sqrt{16\,d^2R_0^2 - 4R_0^2R_\Sigma^2 - 4d^2R_\Sigma^2 + R_\Sigma^4}}, \tag{20}$$

D. Accuracy of the 'Two Hyperbolas' Method

In 'two hyperbolas' method the measurements ξ_1 and ξ_2 are the differential ranges: $\xi_1 = \Delta R_1 = R_1 - R_0$, $\xi_2 = \Delta R_2 = R_2 - R_0$. Then $\sigma_{\xi_1} = \sigma_{\xi_2} = \sigma_R\sqrt{2} = c\cdot\sigma_\tau/\sqrt{2}$. The solutions $\partial x/\partial\xi_1$, $\partial x/\partial\xi_2$, $\partial y/\partial\xi_1$, and $\partial y/\partial\xi_2$ for 'two hyperbolas' method are defined by the following:

$$\frac{\partial k}{\partial \Delta R_1} = 2\frac{\Delta R_1\left(d^2\Delta R_1^2 - 2\Delta R_1^2\Delta R_2^2 + \Delta R_2^2 d^2\right)}{d\left(\Delta R_1^2 - \Delta R_2^2\right)^2} - 2\frac{\Delta R_1 d^2 - 2\Delta R_1\Delta R_2^2}{d\left(\Delta R_1^2 - \Delta R_2^2\right)},$$
$$\frac{\partial x_{tg}}{\partial \Delta R_1} = \frac{\partial k}{\partial \Delta R_1}\Big/2 \pm \frac{\frac{\partial k}{\partial \Delta R_1}\frac{k}{2} + \frac{\Delta R_1\Delta R_2^2}{d^2}}{2\sqrt{\frac{k^2}{4} - \left(\frac{d^2}{4} - \frac{\Delta R_1^2\Delta R_2^2}{4d^2}\right)}},$$
$$\frac{\partial k}{\partial \Delta R_2} = -2\frac{\left(\Delta R_2 d^2 - 2\Delta R_2\Delta R_1^2\right)}{d\left(\Delta R_1^2 - \Delta R_2^2\right)} - 2\frac{\Delta R_2\left(d^2\Delta R_1^2 - 2\Delta R_1^2\Delta R_2^2 + \Delta R_2^2 d^2\right)}{d\left(\Delta R_1^2 - \Delta R_2^2\right)^2},$$
$$\frac{\partial x_{tg}}{\partial \Delta R_2} = \frac{\partial k}{\partial \Delta R_2}\Big/2 \pm \frac{\frac{k}{2}\frac{\partial k}{\partial \Delta R_2} + \frac{\Delta R_2\Delta R_1^2}{d^2}}{2\sqrt{\frac{k^2}{4} - \left(\frac{d^2}{4} - \frac{\Delta R_1^2\Delta R_2^2}{4d^2}\right)}},$$

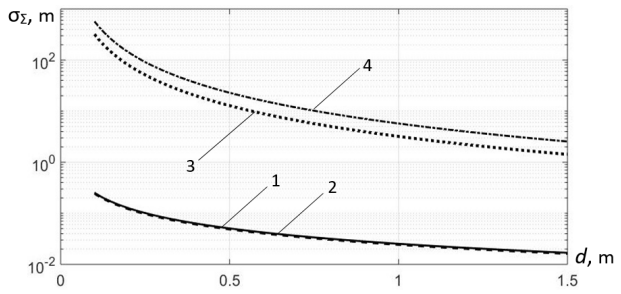

Fig. 6. Root mean square errors of coordinate estimation dependence from the baseline d for different methods: 1 – 'Two circles'; 2 – 'Circle and hyperbola'; 3 – 'Circle and ellipse'; 4 – 'Two hyperbolas'.

$$\frac{\partial y_{tg}}{\partial \Delta R_1} = \pm \left[\frac{\frac{d^2}{\Delta R_1^3}\left[\left(d/2 - x_{tg}\right)^2\right]}{\sqrt{\left(\frac{d^2}{\Delta R_1^2} - 1\right)\left(x_{tg}^2 - x_{tg\ 1,2} d + \frac{\Delta R_1^2}{4}\right)}} - \frac{\left[\left(\frac{d}{\Delta R_1}\right)^2 - 1\right] \cdot \left[\left(\frac{d}{2} - x_{tg}\right)\frac{\partial x}{\partial \Delta R_1}\right] - \frac{\Delta R_1}{2}}{\sqrt{\left(\frac{d^2}{\Delta R_1^2} - 1\right)\left(x_{tg}^2 - x_{tg} d + \frac{\Delta R_1^2}{4}\right)}} \right],$$

$$\frac{\partial y_{tg}}{\partial \Delta R_2} = \pm \frac{\left(\frac{d^2}{\Delta R_1^2} - 1\right)\left[\left(x_{tg} - \frac{d}{2}\right)\frac{\partial x_{tg}}{\partial \Delta R_2}\right]}{\sqrt{\left(\frac{d^2}{\Delta R_1^2} - 1\right)\left(x_{tg}^2 - x_{tg} d + \frac{\Delta R_1^2}{4}\right)}}. \quad (21)$$

In Fig.6 the dependence of coordinate root mean square error for presented methods from the baseline is shown, calculated by (18)-(21), where $\sigma_\Sigma = \sqrt{\sigma_x^2 + \sigma_y^2}$. The following system parameters were accepted: range between receiver and target 5 m, effective signal baseband $\Delta f_{\text{eff.}} = \Delta\omega_{\text{eff}} / 2\pi =$ 4 GHz, detection probability $P_D = 0.9$, and probability of false alarm $P_{FA} = 10^{-6}$. The dependence of P_D from P_{FA} and from the average energy-to-noise ratio q was obtained in [14] for the case of signal detection with random amplitude and phase:

$$P_D = P_{FA}^{1/(1+q^2/2)} \quad (22)$$

From (22) follows the threshold signal-to-noise ratio required for detection with probability P_D for a given false alarm probability P_{FA}

$$q_{out} = \sqrt{2 \cdot \left(\frac{\log_{10} P_{FA}}{\log_{10} P_D} - 1\right)} \quad (23)$$

In the considered case $q_{out} = 16.13$. As we can see from the Fig.6, the root mean square errors of coordinate estimation in 'circle and ellipse' and 'two hyperbolas' methods in the case of small baseline are much higher than in other methods. In cases where the two curves of constant range intersect at only a shallow angle, the large errors in directions close to the tangents to those lines dominate the errors. Indeed, in case of small baseline the angle between two curves in the intersection point is very small. Therefore, for the later sections of this paper 'circle and ellipse' and 'two hyperbolas' methods are not considered for coordinate estimation.

The 'Two circles' and 'circle and hyperbola' methods, on the other hand, have acceptable accuracy of coordinate measurement even in the case of small baseline because the lines of constant range are closer to being orthogonal.

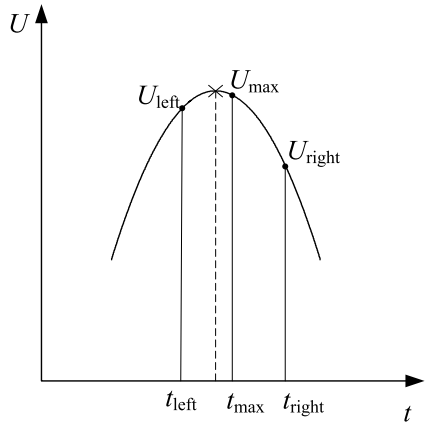

Fig. 7. Signal interpolation based on three points. Signal in the area of the maximum: U – signal amplitude, t – time, U_{max} – maximum sample value, U_{left} and U_{right} – neighbouring samples values.

V. Interpolation of the Reflected Signal Envelope and Rejection of Phantom Target

Because of sampling in most cases the maximum signal sample does not coincide with the center of the signal. Therefore, in order to achieve better accuracy of measurement we shall go back a stage in the processing and consider how the range measurements can best be estimated from the signal envelope. The classical approach to interpolation is to construct a polynomial of order N that passes through the $N+1$ known samples; this polynomial is unique [15]. In Fig. 7 the signal envelope interpolation is based on three points is shown. We will use the second-order approximation of the signal envelope:

$$F(t) = a_2 t^2 + a_1 t + a_0 \quad (24)$$

The center of the signal can be found by placing three values of the $F(t)$ near its maximum in (24) and solving the equation $dF(t)/dt = 0$.

The occurrence of phantom target marks in multiple targets environment was discussed in Section III and illustrated in Fig. 4 for the case of two targets. The number of potential false correlations rises sharply with increasing number of targets. The possible ways to exclude false measurements are, firstly, to increase the number of positions and, secondly, to use the different methods, but measure the target coordinates from the same positions, for example by comparing the set of potential positions obtained by using both the 'circle/circle' and the 'circle/hyperbola' methods. Let us consider the situation when three sensors are used to measure distance to two or more targets. The coordinates of targets are estimated using range measurements (circles) from two side transceivers. The third

transceiver is used to select the targets located at the correct distances from this central transceiver.

In multiple targets environment the central channel can detect another object in other azimuth position at the same range. Instead of location of the areas of intersection of lines of constant range, we should identify the positions of target marks [12]. In this case two point groups are needed: the first vector which is the result of 'circle and circle' method and the second vector which is the result of 'circle and hyperbola' method. Two point vectors are defined by the following:

$$\vec{G}_1 = \begin{bmatrix} \vec{r}_1^{(1)} \\ \vec{r}_2^{(1)} \\ \cdots \\ \vec{r}_{N1}^{(1)} \end{bmatrix} = \begin{bmatrix} x_1^{(1)} & y_1^{(1)} \\ x_2^{(1)} & y_2^{(1)} \\ \cdots & \\ x_{N1}^{(1)} & y_{N1}^{(1)} \end{bmatrix},$$
$$\vec{G}_2 = \begin{bmatrix} \vec{r}_1^{(2)} \\ \vec{r}_2^{(2)} \\ \cdots \\ \vec{r}_{N2}^{(2)} \end{bmatrix} = \begin{bmatrix} x_1^{(2)} & y_1^{(2)} \\ x_2^{(2)} & y_2^{(2)} \\ \cdots & \\ x_{N2}^{(2)} & y_{N2}^{(2)} \end{bmatrix}. \quad (25)$$

With the increase in the number of targets the dimensions of vectors G_1 and G_2 increase sharply [10]. In 'circle and circle' method the dimension of G_1 is equal to N^2, in 'circle and hyperbola' method the dimension of G_2 is equal to $2 \cdot N^3$, where N is number of targets identified in the central channel.

Targets are located on the intersections of uncertainty areas. In order to separate real and phantom targets we should choose all combinations of elements of the first and the second vector and calculate the Euclidean distances between them:

$$\varepsilon_{ij} = \sqrt{\left(x_i^{(1)} - x_j^{(2)}\right)^2 + \left(y_i^{(1)} - y_j^{(2)}\right)^2}. \quad (26)$$

In (26) i is the point number from the first vector, j is the point number from the second vector. As target locations we should choose the vector elements $\vec{G}_1$ ($\vec{G}_2$) where:

$$\varepsilon_{ij} < \rho_{ij}. \quad (27)$$

In (27) ρ_{ij} is the radius of uncertainty of $\vec{r}_i^{(1)}, \vec{r}_j^{(2)}$, it depends on the range to the target and the accuracy of measurements.

Note that even this technique will not be infallible when the density of 'real' targets becomes too great. This method of estimating position is therefore most suited to cases where the target density is low, such as is the case in the 'height' direction, and to continue to rely on a relatively-narrow angular resolution of a directional antenna array.

Other researchers discussed different solutions of the problem of correct data association, including nearest neighborhood method and the technique based on the method of least squares with subsequent trajectory processing [16].

VI. Experimental Results With One Point Target

The purpose of this section is the experimental verification of the effect of various parameters on the accuracy of determining the coordinates of the point target. The experimental system was based on Keysight FieldFox N9918A Vector Network Analyzer (VNA), its output signal was transferred using up and down converters to the low terahertz range with

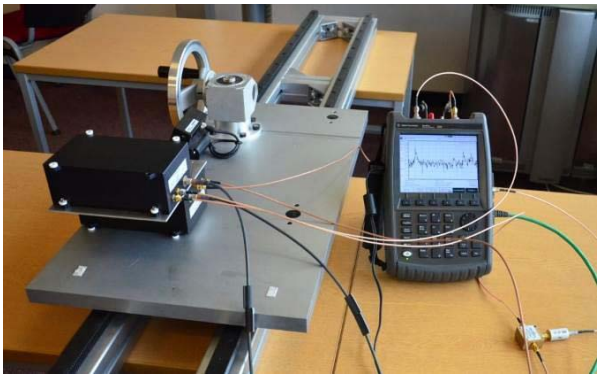

Fig. 8. Experimental system.

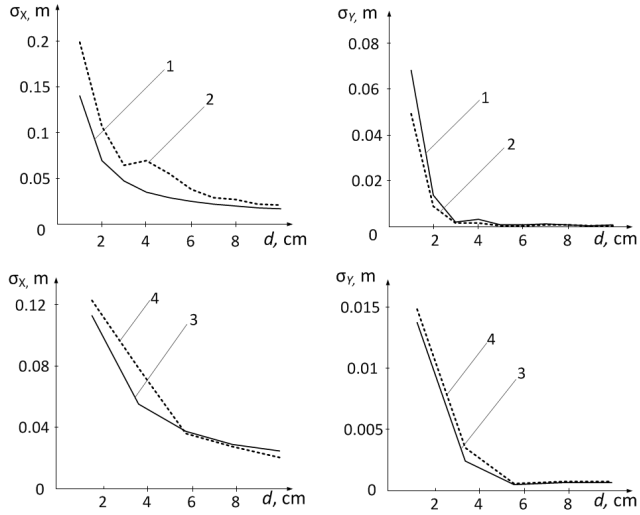

Fig. 9. Root mean square errors of coordinate estimation dependance on the baseline: 'Two circles' method: 1 – theory, 2 – experiment; 'Circle and hyperbola' method: 3 – theory, 4 – experiment.

the central frequency of 300 GHz and bandwidth from 2 GHz to 18 GHz. Linear and vertical positioners allow moving the transceivers by a predetermined distance, thereby creating a virtual sensors array. The manually operated horizontal positioner has positioning precision of 0.1 mm and 3 m travel range. The computer-controlled vertical positioner has positioning precision of 5 μm and 10 cm travel range in vertical direction. The antenna beamwidth (on the main lobe level of -3 dB) was 10 degrees in both the azimuth and the elevation planes. In Fig. 8 the experimental system is shown.

In the first stage, we defined how the length of the baseline affects the error of coordinate measurement. As can be seen from Fig. 6, this parameter plays an important role in overall system accuracy. Fig. 9 shows the dependence of coordinates x and y root mean square errors for 'circle and circle' and 'circle and hyperbola' methods from the baseline. Aluminum bars (4.5 cm × 4.5 cm × 1.0 cm) were used as point targets; the signal bandwidth was 4 GHz; the results of the experiments for each receiver position were averaged over 100 samples.

The experimental results show that in case of 5-10 cm baseline the root mean square error of x coordinate estimation varies from 2 cm to 3 cm. If the baseline becomes

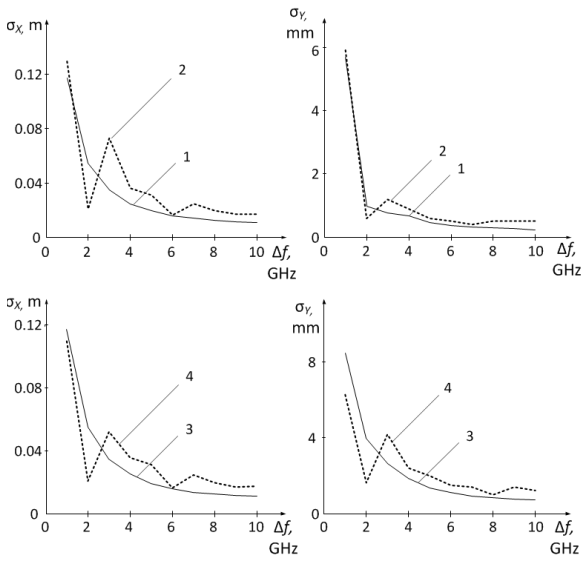

Fig. 10. Root mean square errors of coordinate estimation dependance on the bandwidth: 'Two circles' method: 1 – theory, 2 – experiment; 'Circle and hyperbola' method: 3 – theory, 4 – experiment.

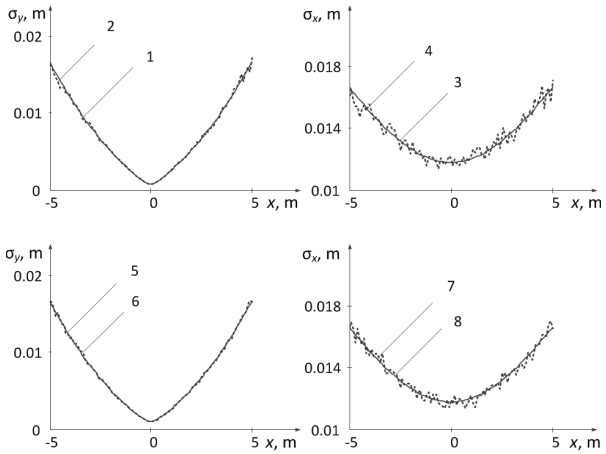

Fig. 11. Root mean square errors of coordinate estimation dependance on the target abscisae: 'Two circles' method: 1, 3 – theory, 2, 4 – computer simulation; 'Circle and hyperbola' method: 5. 7– theory, 6. 8 – computer simulation.

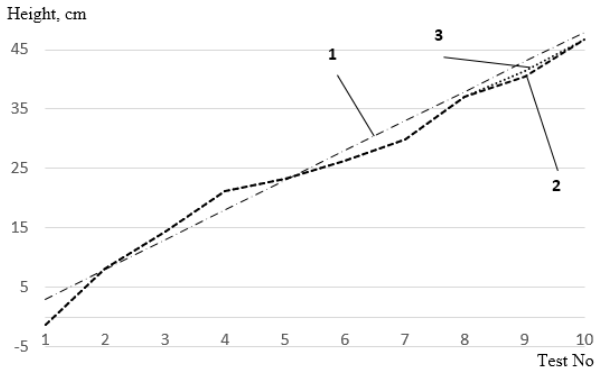

Fig. 12. The estimated height: 1 – theory, 2 – experimental results using 'two circles' method: 3 – experimental results using 'circle and hyperbola' method.

less than 5cm, the root mean square error of x coordinate estimation rises to become 2-4 times higher than the range resolution (3.75 cm). The system with the baseline of more than 10 cm has acceptable coordinate measurement accuracy.

The second parameter that affects the accuracy of measurements is the signal bandwidth. Increasing the bandwidth of the signal reduces the potential error of coordinate measurement, defined by $\sigma_\tau = 1/(q_{\text{out}} \cdot \Delta\omega_{\text{eff.}})$. Fig. 10 shows the dependence of theoretical and experimental accuracy of coordinate measurements on the signal bandwidth. The baseline was 20 cm and the distance to the target was 5 m. From the analysis of Fig. 10 follows, that the system with the bandwidth of more than 4 GHz has acceptable coordinate measurement accuracy.

As can be seen from the graphs, the experimental results are broadly consistent with the theoretically calculated, except for the area around 3 GHz. We should note that at this frequency the target size is approximately equal to the range resolution (5 cm) and it is likely that the range measurements are being affected, at second-order, by resonance effects.

The third parameter, which influences the accuracy of the measurement, is the azimuthal displacement of the target. Fig. 11 shows the dependence of root mean square errors of coordinates x and y measurement on the target abscissa x_{tg} for 'circle and circle' and 'circle and hyperbola' methods, using computer simulation. The distance to the target y_{tg} is 5 m, the baseline is 40 cm (distance between the positions 20 cm), signal bandwidth of 4 GHz, and q_{out} was equal to 16.13. As expected, the increase in the r.m.s. error corresponds to the increase of $\sqrt{2}$ in the slant range to the target as it moves from 0m to $\pm$5m cross-range distance.

From this figure we can see that root mean square errors of coordinate measurement have a minimum when the target is placed normal to the baseline.

At the end of the section, we present the results of the experiment of measuring the height of a corner reflector at different height. The distance between radar and the corner reflector is 5 m; the baseline is 36 cm, and the bandwidth is 16 GHz (range resolution 9.4 mm). The results of experiments were averaged over 20 samples. They are graphically presented in Fig. 12 and show good agreement between the theory and the experiment.

For the practical application of the methods considered in this paper it is necessary that the height resolution to be less than the height of the object, that is, we could identify the reflective points and determine the coordinates of the highest of them. Therefore, it is necessary to analyze the application of these methods in the case of distributed targets.

VII. Distributed Target

A distributed target is a target having dimensions bigger than the range or angle resolution of the radar. There are two types of distributed targets – volume-distributed and surface-distributed targets [17]. A volume-distributed target is a target having a volume and distributed over the range and angle. The examples of surface-distributed targets are road, water surface, grass-covered surface, etc.

a) *b)*

Fig. 13. Half-height mannequin (a) and a mannequin dressed in a high visibility jacket (b)

A distributed target does not usually have a uniform reflectivity, but has some areas with the strongest reflections. The reflection point is a surface area reflecting signal in the directional of the receiver. Usually the reflection point is a corner reflector or a flat surface perpendicular to the direction of the electromagnetic wave. Each distributed target has several reflection points. If the resolution of the system is larger or equal to the size of the target, the time domain signal reflected from a target can be considered as one reflection which is the superposition of reflections from a number of the single reflection points. If the resolution of the system is smaller than the size of the target, the reflected signal consists of a number of reflection points which can be used to estimate the size of the target. In this case, the target has a range profile and it can be identified by this profile.

To verify the method of height measurement, the experiments were carried out with a distributed target. A half-height mannequin was chosen as a target (Fig. 13), because in order to illuminate a full-height mannequin the distance to the object should exceed 10 m, what was difficult to provide for the conditions of the experiment. The mannequin height was 79 cm and the range to the mannequin was approximately 6 m.

The number of the reflection points depends on the target shape, the wavelength, the range and angle resolutions, and the observation angle. Furthermore, when we consider the reflection from a mannequin, this number depends on the type of clothing. Small torso turns can lead to a significant change in the distribution of reflecting points. As was shown by our measurements, the reflection from a mannequin without clothes is very small, which makes difficult to measure its height at distances greater than several meters. The reflection from a dressed mannequin was much higher (Fig. 14).

Fig. 14 shows that a practical target, even one such as the mannequin with no obvious significant reflectors, shows the small group of approximately-discrete reflectors which the trilateration method requires for it to be able to work.

Table I shows the result of measuring the height of the reflecting points of the mannequin (Fig. 13a) when the signal bandwidth was 16 GHz. The reflecting points are sorted

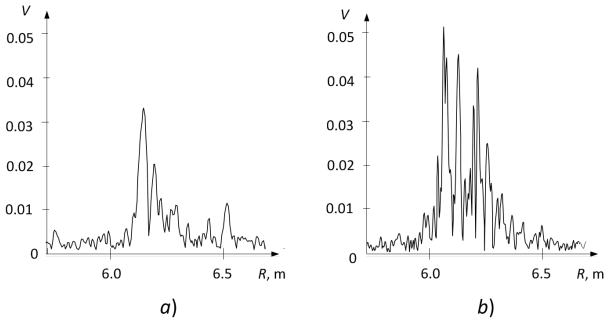

Fig. 14. Amplitude of the signal with 16 GHz bandwidth (in volts), reflected from a mannequin (a) and from a mannequin dressed in a high visibility jacket (b).

TABLE I

THE ESTIMATED HEIGHT OF REFLECTION POINTS, CM

	Reflection Point Number	
	1	2
'Two circles' method	38.6	57.9
'Circle and hyperbola' method	35.6 45.2	57.9 23.1

TABLE II

THE ESTIMATED HEIGHT OF REFLECTION POINTS, CM

	Reflection Point Number				
	1	2	3	4	5
'Two circles' method	24.6	31.9	46.5	52.3	55.9
'Circle and hyperbola' method	24.6 56.4	31.9 49.1	34.5 46.5	28.7 52.3	26.1 55.9

in ascending order of height. As can be seen from the Fig. 14a, the mannequin has two clearly distinguishable reflection points; their heights correspond to jugular depression and abdomen. The maximum height of the reflecting point was 57.9 cm. The signal reflected from the head was weak, that did not allow us to measure the total height of the mannequin. 'Circle and hyperbola' method yields two results, one of which is false, what is evident from a comparison with the results of the first method ('two circles').

Table II shows the result of measuring the height of the reflecting points when the mannequin was dressed in reflective clothing (Fig. 13b). In this case, we were able to identify five reflecting points, as shown in Fig. 14b. The reflecting points in the table are sorted in ascending order of height. It is evident that in the case of a distributed target there is no direct correlation between the distance to the reflecting point and its height. As can be seen from the table, the maximum height of the reflecting point was 55.9 cm, which corresponds to the height of a chin.

VIII. CONCLUSION

In this paper radar methods to determine the coordinates of road objects (distance and height) have been investigated. Knowledge of these parameters is essential to enhance the safety of driving. To solve this problem we have applied low-THz radar trilateration approach.

The expressions were obtained, allowing calculating the coordinates of targets using various methods of radar trilateration. The influence of the system parameters (baseline and bandwidth) on the accuracy of measurement was analyzed. Experimental results are in good agreement with theoretical calculations; they confirmed the possibility of target coordinate measurement with high accuracy. When distance to the target was 5 m, the height can be measured with the accuracy of a few centimeters. It was shown that 'two circles' and 'circle and hyperbola' methods have acceptable accuracy of coordinate measurement even in the case of small baseline.

In order to separate real and false targets in multiple targets environment, two radar trilateration methods are needed for ambiguity resolution. A method for filtering the false targets was considered in the paper.

Finally, we estimated what signal parameters allow separation of two reflection points with different height and equal range. The obtained assumptions were verified experimentally by measuring the height of a distributed target (mannequin). The results confirm the applicability of this approach to measure the height of distributed road objects, including pedestrians. The conducted research can be used in the development of autonomous or semi-autonomous cars, as well as to improve driving safety.

Now that the potential of height-finding has been established, future work can and will, of course, investigate the performance which is obtainable in more complex environments, where clutter and interference may be present.

ACKNOWLEDGMENT

The authors would like to acknowledge the helpful comments made by the anonymous reviewers, which have enabled us significantly to improve this paper.

REFERENCES

[1] J. Hasch, "Driving towards 2020: Automotive radar technology trends," in *Proc. IEEE MIT-S Int. Conf. Microw. Intell. Mobility*, Heidelberg, Germany, Apr. 2015, pp. 1–4.

[2] H. Ritter and H. Rohling, "Pedestrian detection based on automotive radar," in *Proc. IET Int. Conf. Radar Syst.*, Edinburgh, U.K., Oct. 2007, pp. 1–4.

[3] C. Waldschmidt and H. Meinel, "Future trends and directions in radar concerning the application for autonomous driving," in *Proc. 44th Eur. Microw. Conf.*, Rome, Italy, Oct. 2014, pp. 171–172.

[4] S. Heuel and H. Rohling, "Pedestrian recognition in automotive radar sensors," in *Proc. 14th Int. Radar Symp. (IRS)*, Dresden, Germany, vol. 2, Jun. 2013, pp. 732–739.

[5] A. Bartsch, F. Fitzek, and R. H. Rasshofer, "Pedestrian recognition using automotive radar sensors," *Adv. Radio Sci.*, vol. 10, pp. 45–55, Sep. 2012.

[6] T. Wagner, R. Feger, and A. Stelzer, "Modification of DBSCAN and application to range/Doppler/DoA measurements for pedestrian recognition with an automotive radar system," in *Proc. Eur. Radar Conf. (EuRAD)*, Paris, France, Sep. 2015, pp. 269–272.

[7] J. Wenger, "Future trends in automotive radar/imaging radar," in *Proc. 28th Eur. Microw. Conf.*, Amsterdam, The Netherlands, Oct. 1998, pp. 636–641.

[8] M. Schneider, "Automotive radar—Status and trends," in *Proc. German Microw. Conf. (GeMiC)*, Ulm, Germany, 2005, pp. 144–147.

[9] J. F. Cline, "Multilateration error ellipsoids," *IEEE Trans. Aerosp. Electron. Syst.*, vol. AES-14, no. 4, pp. 665–667, Jul. 1978.

[10] H. Rabe, E. Denicke, G. Armbrecht, T. Musch, and I. Rolfes, "Considerations on radar localization in multi-target environments," *Adv. Radio Sci.*, vol. 7, pp. 5–10, May 2009.

[11] V. S. Chernyak, *Fundamentals of Multisite Radar Systems: Multistatic Radars and Multistatic Radar Systems*. Boca Raton, FL, USA: CRC Press, 1998.

[12] A. V. Myakinkov and D. M. Smirnova, "Measurement of coordinates of the targets placed behind of radio-transparent barrier with multi-static ultra-wide band radar," in *Proc. 5th Int. Conf. Ultrawideband Ultrashort Impulse Signals*, Sevastopol, Ukraine, Sep. 2010, pp. 147–149.

[13] A. P. Sage and J. L. Melsa, *Estimation Theory With Applications to Communications and Control*. New York, NY, USA: McGraw-Hill, 1971.

[14] S. M. Kay, *Fundamentals of Statistical Signal Processing: Detection Theory*. Upper Saddle River, NJ, USA: Prentice-Hall, 1998.

[15] S. V. Vaseghi, *Advanced Digital Signal Processing and Noise Reduction*. 2nd ed. Hoboken, NJ, USA: Wiley, 2000.

[16] F. Folster and H. Rohling, "Data association and tracking for automotive radar networks," *IEEE Trans. Intell. Transp. Syst.*, vol. 6, no. 4, pp. 370–377, Dec. 2005.

[17] I. Immoreev, "Feature detection in UWB radar signals," in *Ultra-Wideband Radar Technology*, J. D. Taylor, Ed. Boca Raton, FL, USA: CRC Press, 2001, pp. 33–58.

Sergei Shishanov received the M.Eng. degree in radiotechnology from Nizhny Novgorod State Technical University n.a. R.E. Alekseev, Russia, in 2012. In 2010, he was with electronic and IT industry in Russia. He has authored three papers. The scientific area of his research activity is automotive radar and signal processing algorithms.

Aleksandr Bystrov received the M.Eng. degree in electronics from Moscow Institute of Electronic Technology in 1982 and the Ph.D. degree in electronics from National Research University of Electronic Technology, Moscow, Russia in 2012. From 1983 to 2012, he was with electronic and IT industry in Russia and Lithuania. Since 2012, he has been a Research Fellow with the Microwave Integrated System Laboratory, University of Birmingham. He has authored over 30 papers and six inventions. His research interests include radar, sonar, and signal processing algorithms.

Edward G. Hoare (SM'99) received the Ph.D. degree from the School of Electronic and Electrical Engineering, University of Birmingham, with a focus on his research over-the-horizon radars. He undertook an apprenticeship at The Royal Radar Establishment, College of Electronics, Malvern, U.K., and, after some time in industry.

Over the past 20 years, he has provided sensor, antenna, and millimeter-wave radar consultancy to Jaguar Cars, Land Rover, and The Ford Motor Company, delivering over 60 technical reports on millimeter-wave antennas, radar, signal processing, and associated topics. He holds a number of patents in automotive radar and sensors. His research interests include radar systems and antennas covering frequencies from 2 MHz to over 1 THz, including non-cooperative bistatic radar, forward scatter maritime radar, radar acoustic sounding, millimeter-wave automotive radar, and terahertz radar.

He is currently a Senior Research Fellow with the Microwave Integrated Systems Laboratory, University of Birmingham. He is a member of the Institution of Engineering and Technology, and was a member of the European Automotive Radar Standards Group.

Andrew Stove joined the Microwave Integrated System Laboratory in 2015 in an honorary capacity after 18 years with Thales U.K. and 16 years with Philips. One area of his work has been on continuous wave radars using frequency- and noise-modulation for naval navigation, to evade interception by electronic surveillance receivers, for smart ammunition and for automotive radars. Other areas of work have been the design and testing of airborne radars for maritime surveillance and airborne early warning radars, target identification, particularly using Doppler techniques and bistatic radars.

Marina Gashinova received the M.Sc. degree in math from Saint Petersburg State University in 1991 and the Ph.D. degree in physics and mathematics from Saint Petersburg Electrotechnical University, Russia, in 2003. In 2006, she joined the Microwave Integrated System Laboratory, University of Birmingham, where she is currently a Senior Lecturer in radar and RF sensors, leading the research group on passive and active bistatic radar, terahertz radar imaging, and automotive sensors. She has authored or co-authored over 80 publications in peer-reviewed journals and conferences and presenter of several invited and focused talks on forward scatter radar at international conferences, workshops, and seminars.

Mikhail Cherniakov graduated from Moscow Technical University in 1974 and received the Ph.D. degree in 1980 and the D.Sc. degree in 1992. He was a Full Professor with Moscow Technical University in 1993. In 1994, he was a Visiting Professor with the University of Cambridge and in 1995 he moved to The University of Queensland, Australia. In 2000, he joined the School of EESE, Birmingham. He founded the Microwave Integrated Systems Laboratory that is the biggest radar research team in UK Universities. He is currently a Chair in aerospace and electronic systems with the University of Birmingham, U.K., with over 40 years' experience on the Research and Development in radar systems. His research interests are in bistatic and multistatic radar, radars with phased array, and automotive and short range sensors. He has authored or editor or co-authored three books, and has over 250 peer-reviewed publications.

Thuy-Yung Tran received the B.Eng. degree in electronic and electrical engineering from University of Birmingham in 1999. After the graduation, she joined the Jaguar Land Rover Automotive PLC, where she works on the development of semi-autonomous car technology. She is responsible for the development of blind spot monitoring, wade aid, surface identification systems and new sensor technologies, including low-terahertz radar imaging.

Nigel Clarke received the B.Sc. degree in electrical engineering from Loughborough University in 1980 whilst undertaking an apprenticeship with Lucas Aerospace. Following a few years providing product support on gas turbine electronic control modules, he joined Jaguar Cars in 1983. He was a member of the Programme for European Transport with the Highest Efficiency and Unprecedented Safety Technical Committee. He then went on to lead a number of EC Framework and U.K. Government funded projects in the area of active safety being pivotal in the development of blind spot monitoring on JLR products and also wade aid. His main responsibility has been the development of off-road technology at Land Rover, being responsible for the development of terrain response, and all-terrain progress control. His brief has now been extended to include research on sensing systems for autonomous on and off-road vehicles.